

Indium segregation in ultra-thin In(Ga)As/GaAs single quantum wells revealed by photoluminescence spectroscopy

Y. Maidaniuk¹, R. Kumar², Yu. I. Mazur¹, A. V. Kuchuk^{1*}, M. Benamara¹, P. M. Lytvyn³, G. J. Salamo¹

¹*Institute for Nanoscience & Engineering, University of Arkansas, Fayetteville, AR 72701,
United States*

²*Department of Electrical and Electronics Engineering, Birla Institute of Technology and
Science, Pilani, Pilani-333031, India*

³*V. Lashkaryov Institute of Semiconductor Physics, National Academy of Sciences of Ukraine,
Kyiv 03680, Ukraine*

Abstract

An non-destructive approach is described that is applicable for studying the In-segregation phenomena in ultra-thin In(Ga)As/GaAs nanostructures grown by molecular beam epitaxy (MBE). The proposed method utilizes only the experimental photoluminescence (PL) spectroscopy data and the effective bandgap simulation of specially designed ultra-thin In(Ga)As/GaAs nanostructures. On the example of InAs and In_{0.25}Ga_{0.75}As quantum wells with thicknesses of 1 monolayer (ML) and 4 MLs, respectively, a good correlation for the In segregation coefficient obtained from the proposed method and STEM (scanning transmission electron microscope) Z-contrast cross-section imaging is demonstrated. However, PL has a significant advantage over STEM of being non-destructive, reliable and rapid technique for measuring multiple samples or large areas. Furthermore, tuning of In segregation in ultra-thin In(Ga)As/GaAs nanostructures, as well as the possibility of modifying and controlling the In depth-distribution profile by the change of growth temperature or the thickness of the low-temperature GaAs capping layer, are additionally demonstrated. A detailed analysis of indium segregation allows to design and precise growth of ultra-thin In(Ga)As/GaAs nanostructures for lasers, solar cells, and infrared photodetectors.

*Corresponding author: kuchuk@uark.edu

The ultra-thin In-containing group III-arsenide(nitride) quantum wells (QWs) are in the focus of researchers in the last years due to their unique properties and the plethora of potential applications. In particular, the 2D In(Ga)N layers sandwiched in a GaN matrix are promising for the fabrication of single-photon emitters¹ and light emitting devices operating within the infrared and ultraviolet regions.^{2,3} The other application of ultra-thin In(Ga)As/GaAs QWs includes lasers,⁴ solar cells,⁵ and infrared photodetectors.⁶ Recently, a sub-monolayer (SML) quantum dot (QD) cascade mid-infrared photodetector grown on GaAs was proposed as a promising replacement for the more matured QD-based devices.⁷ One of the advantages of using sub-ML growth is the complete absence of a wetting layer that is responsible for carrier trapping, which usually results in diminished device performance.⁸ At the same time, the growth of ultra-thin InGa(As,N) QWs structures with predictable properties is still challenging.⁹⁻¹⁴ The chemical ordering, which limits the composition of 1 ML In(Ga)N QW to In content of 25%,² severely narrows the tunability of ultra-thin InGaN QWs-based emitters. Moreover, random fluctuations of the indium concentration leads to a decrease in the radiative recombination and consequently the efficiency drop in InGaN/GaN-based light emitting diodes.¹⁵

Different phenomena occur during the growth of InGaAs layers since the bonding nature of In atoms in the GaAs and GaN matrices are different. The lateral and vertical indium segregation,^{16,17} In-rich agglomerations,¹⁸ and In redistribution¹⁹ are observed during the capping of the ultra-thin InAs layers by GaAs. In general, the segregation which is related to the near-equilibrium established between the volatile group III species on the growth surface and the crystal bulk is one of the critical parameter which influence on the In depth-distribution in InGaAs thin films.²⁰

Indium segregation in InGaAs/GaAs system was widely studied both experimentally and theoretically.^{21,22} The first theoretical model based on the thermodynamical equilibrium proposed by Moison, *et al.*²³ failed to explain the experimental results of In segregation as a function of growth temperature. The second empirical model was developed by Muraki, *et al.*,²⁴ where the quantitative analysis of In segregation was performed by using the secondary ion mass spectrometry (SIMS) to explain the photoluminescence (PL) data for relatively thick InGaAs/GaAs QWs. It should be noted that the Muraki's model provides a better agreement with experimental data obtained by using the X-ray diffraction (XRD), scanning transmission electron microscopy (STEM) and SIMS techniques.²⁵⁻²⁷ Moreover, this model shows that the growth temperature is the main factor that determines the segregation of In in InGaAs/GaAs structures.

In this paper, we report a non-destructive approach for studying the In-segregation phenomena in the ultra-thin In(Ga)As/GaAs QWs grown by molecular beam epitaxy (MBE). The proposed method utilizes a design of GaAs/In(Ga)As/GaAs structures and experimental PL data supported by effective bandgap simulation. STEM Z-contrast cross-section imaging was carried out to validate the accuracy of proposed non-destructive PL technique, which revealed the In depth-distribution as a result of In segregation during the capping of ultra-thin In(Ga)As layers by GaAs. Additionally, the possibility of modifying the In depth-distribution profile by tuning the In(Ga)As growth temperature or the thickness of the low-temperature GaAs capping layer was demonstrated.

The samples S1-S8 discussed in this work were grown by a conventional MBE technique on semi-insulating GaAs (001) substrates. The growth parameters for each sample are summarized in Table 1. At first, the substrate native oxide was thermally desorbed by heating the substrate at 600°C for 10 minutes under the presence of an As₂ flux. Then, a 500 nm thick GaAs

buffer layer was grown at 580 °C. Subsequently, the substrate temperature was decreased to $T_g^{In(Ga)As}$ for the growth of a single ultra-thin In(Ga)As QW. After the QW deposition, a 10 second growth interruption was introduced followed by the deposition of a low-temperature (LT) GaAs cap layer at $T_g^{In(Ga)As}$. The substrate temperature was then increased to 580°C and a high-temperature (HT) GaAs cap layer was grown. The total thickness of the GaAs cap layer was ~ 50 nm. The two-dimensional (2D) growth was confirmed by reflection high energy electron diffraction (RHEED). The PL measurements were performed at 10 K in a closed-cycle helium cryostat. For the excitation, the 532 nm line from a doubled Nd:YAG laser was used with the power of 2 mW after neutral density filters. The laser beam was focused to a spot with a diameter of $20 \pm 5 \mu\text{m}$. The PL spectra were recorded by SpectraPro 2500i spectrograph. The effective bandgap simulations were obtained by using nextnano software package.²⁸ X-ray diffraction spectra were measured by using PANalytical X'Pert MRD diffractometer equipped with a multilayer focusing mirror, a standard four-bounce Ge (220) monochromator providing a collimated and monochromatic incident $\text{CuK}\alpha_1$ source of radiation ($\lambda = 0.15406 \text{ nm}$), and a Pixel detector. Dark-field STEM images were obtained using a Fischione high-angle annular dark-field imaging (HAADF) detector. The samples were oriented along the [011] and $[0\bar{1}1]$ zone axis.

In order to study the effect of the In depth-distribution on the emission properties of In(Ga)As QWs with the same amount of In content, the following set of single quantum well GaAs/QW/GaAs structures were designed: 1 ML InAs (S1), 2 ML $\text{In}_{0.5}\text{Ga}_{0.5}\text{As}$ (S2) and 4 ML $\text{In}_{0.25}\text{Ga}_{0.75}\text{As}$ (S3) QWs sandwiched in a GaAs matrix, so that each of these QWs has the same total amount of indium that is sufficient to grow 1 ML of InAs (see Table 1). All three samples show a strong and narrow PL peak at ~1.47 eV, with the average full width at half-maximum (FWHM) of $\sim 8 \pm 2 \text{ meV}$ (see Fig. 1). Fluctuation of FWHM of PL peak for samples S1-S3 (see

Table 1) can be related with inhomogeneity of In distribution at nanoscale as well as increase of defect density for thicker QWs. The PL peaks are red shifted with respect to the bulk GaAs band gap energy and therefore, can be attributed to the inter-band e_1-hh_1 transitions in the ultra-thin In(Ga)As single QW. The simulation of the band alignment and of the transition energy for samples S1-S3 were performed using the nextnano 3D simulator, assuming nominal indium content and its depth-distribution in the In(Ga)As QWs (see Table 1). As can be seen in Fig. 1, the simulated (vertical dashed lines) and experimental data are in a good agreement only for sample S1, while the PL peak position and the simulated transition energy for samples S2 and S3 are mismatched of about 30 meV. The PL results in Fig. 1 are in good agreement with the PL energy of 1.46 eV for 1 ML of InAs/GaAs reported by Yuan *et al.*²⁹ and Tran *et al.*³⁰, where an island nature of quantum confinement formation was assumed. Indeed, the In(Ga)As islands with one monolayer height are formed during nominal sub-monolayer growth. Moreover, these islands can preserve their shape after being capped with GaAs.^{31,32} The optical properties of island-based In(Ga)As structures are indistinguishable from those of In(Ga)As QWs with the same amount of indium, since the size of islands and the distance between them is smaller than the exciton Bohr radius.²⁹ However, this cannot explain the results observed for samples S2 and S3, since the thickness of the In(Ga)As QWs for those samples is larger than 1 ML. Moreover, as a result of In depth-distribution in In(Ga)As QWs for samples S2 and S3, the accumulated elastic strain energy does not reach the critical value for islands formation. Therefore, the mismatch between experimentally observed PL and simulated transition energy for samples S2 and S3 can be attributed to either indium segregation and/or desorption during the growth.

X-ray diffraction (XRD) $\omega/2\theta$ spectra were measured across the 004 reflection in order to estimate the In content in ultra-thin In(Ga)As QWs buried in GaAs matrix.^{11,33} The interference

of X-rays scattered from GaAs cap layer and GaAs substrate is observed on the XRD pattern in Fig. 2 as pendellösung fringes surrounding the 004 GaAs Bragg peak. The distance between the satellite peaks on the $\omega/2\theta$ spectra allows calculating the thickness of the GaAs cap layers.^{34,35} In order to calculate the In content the simulation was performed by using the PANalytical X'Pert epitaxy software considering a fully strained GaAs/QW/GaAs system. The structural parameters obtained from XRD curve fitting are tabulated in the inset of Fig. 2. According to these results, the In content and the thicknesses of the $\text{In}_x\text{Ga}_{1-x}\text{As}$ QWs correspond to nominal values. However, it should be noted, that in case of ultra-thin buried layers, the composition and the layer thickness cannot be determined independently by XRD technique.^{36,37} Therefore, the results of XRD curves fitting should be considered as a product of In-composition and the QW-thickness. Nevertheless, it can be concluded that the mismatch in the PL data for samples S1-S3 (see Fig. 1) cannot be explained by desorption of In adatoms during the growth. Consequently, another reason of the observed PL data can be the vertical distribution of In atoms as a result of In segregation during the capping with GaAs. Indeed, from the high-resolution transmission electron microscopy (HRTEM) data and the RHEED intensity analysis we can explicitly conclude on the segregation of In atoms during the growth of the GaAs cap (see Figs. S1-S3). However, the quantitative study of In segregation by XRD, HRTEM and RHEED techniques in case of ultra-thin In(Ga)As/GaAs nanostructures is still challenging.

In order to provide a quantitative analysis of the In segregation for samples S1-S3, we used Muraki model,²⁴ since this model demonstrated a good agreement with experimental data for thick InGaAs/GaAs QWs grown under various conditions.²⁵⁻²⁷ The idea behind the Muraki segregation model assumes that during the growth, some fraction R of indium atoms from the topmost completed layer segregates to the next growing layer. Consequently, the gallium atoms,

which have the higher bonding energy with arsenic, replace segregated In atoms into the layer. It is important to note that only the topmost layer takes part in the segregation process. All the other layers which are located underneath are finalized in terms of indium content distribution. The general formula to calculate the indium content (x_n) in the n -th layer is represented as follows:

$$x_n = \begin{cases} x(1 - R^n), & n < N \\ x(1 - R^N)R^{n-N}, & n > N \end{cases} \quad (1)$$

where x is the nominal indium content, N is the nominal thickness of QW given in MLs, and R is the segregation coefficient. Therefore, in case of 1 ML InAs QW sandwiched in a GaAs matrix, when $R = 0$ (no segregation), the indium content profile has an initially intended shape. The obtained In depth-profiles can be used as an input for the numerical calculation of the conduction and valence band edges of In(Ga)As/GaAs QW structures. Consequently, the effective bandgap E_g^{eff} can be obtained as the inter-band e_1 - hh_1 transition energy for the corresponding structure and the value of R . Figure 3(a) shows the simulation of the effective bandgap energy ($E_{eff} = E_{eff}(x, N, R)$) as a function of continuous variable R for the samples S1, S2, and S3. The x and N are the predefined parameters established before the sample growth. For samples S1, S2, and S3, the indium content and the In(Ga)As nominal layer thicknesses are $x = 1, 0.5, 0.25$ and $N = 1, 2, 4$ MLs, respectively. As can be seen in Fig. 3a, without the In segregation process ($R = 0$), the simulated E_{eff} for the given structures varies from ~ 1.438 to ~ 1.468 eV. On the other hand, for $R > 0.5$ the E_{eff} coincide for all three structures S1-S3. However, the simulated results of E_{eff} correlate with the experimental PL data of sample S1-S3 (horizontal dashed grey line) only for $R \sim 0.83$. Therefore, by using Eq. 1 with $R \sim 0.83$ and the nominal indium content (x) and thickness (N), we calculated the In depth-profiles for samples S1-S3 (see Fig. 3b). It should be

noted that an error in the experimental x and N lead to the error in the calculated In segregation coefficient R . Accordingly, the segregation coefficient will be in the range of $R = 0.83 \pm 0.03$, by introducing the error of 2% in nominal composition and thickness of In(Ga)As QW.

The STEM analysis was performed to prove the In depth-profiles, and consequently the In segregation coefficient determined by PL technique. The actual STEM Z-contrast cross-section images are shown as insets in Fig. 4, where the InGaAs QW can be seen as a brighter region due to the indium incorporation in that area. The data (open grey circles) represent the intensity extracted from the STEM images averaged over the area (white box) shown in the insets. Lenz *et al.* used a similar approach for sub-monolayer InAs/GaAs superlattice structures.¹⁸ The zero-coordinate position is set to coincide with the first interface of the In(Ga)As QW. The experimental STEM data were fitted (solid step-like lines in Fig. 4) according to the segregation model described by equation (1) using the least squares method. The In segregation coefficients that were extracted from the best fit are 0.85 and 0.81 for samples S1 and S2, respectively. The obtained values are in a good agreement with the segregation coefficient $R \sim 0.83 \pm 0.03$ found using the PL data analysis. Therefore, we can conclude, that the experimental PL data for samples S1-S3 (see Fig. 1) can be explicitly explained by In segregation during the GaAs capping process with the In segregation coefficient $R \sim 0.83 \pm 0.03$. Moreover, it is shown, that unlike the STEM, which is a destructive, expensive, and time-consuming process, the PL technique is a reliable alternative to probe the indium depth-profiles (indium segregation) in ultra-thin In(Ga)As/GaAs QW structures.

The growth temperature is one of the most influential parameters that affects the level of In segregation for In-containing III-arsenide structures. Therefore, the samples with 1 ML InAs/GaAs QW grown at 460 °C (S1), 420 °C (S4) and 380 °C (S5) were studied in order to

demonstrate the capability of proposed PL technique to probe the indium depth-distribution profile. The simulated effective bandgap shown in Fig. 3a can be reused in this case since the nominal QW thickness and the In content are the same as for the sample S1. Figure 5a shows the normalized low-temperature PL spectra for samples S1, S4, and S5. Despite the fact that the nominal QW thickness and the In content are the same for all samples, the blue shift in the PL peak position testify on the influence of growth temperature on the In segregation phenomena. Indeed, by using the simulation describe above (see Fig. 3a), it is found that the obtained In segregation coefficients are in a range of ~ 0.62 to ~ 0.83 when the growth temperature was increased from 380 to 460 °C. The resulted In depth-profiles for samples S1, S4 and S5 are shown in Fig. 5c.

The impact of the growth design of InGaAs/GaAs QWs on the In depth-profile was also tested by changing the thickness of LT GaAs layer (l_{cap}). The set of samples S6, S7, and S8 is the repetition of the previous set S1, S4, and S5, with the decreased l_{cap} from 35 ML to 4 ML. The PL spectra for these samples are shown in Fig. 5b. The PL peaks for corresponding growth temperatures are blue shifted as the thickness of the LT GaAs cap decreases. A similar growth was studied by Ilg *et al.*²⁵, where the authors reported a redshift in the PL peak for thinner LT GaAs cap layer. In the present work, the opposite result was observed. To explain this observation, the indium depth profiles for each of the structures were modified according to the growth parameters. Specifically, we assume that the In segregation coefficients for samples S6, S7, and S8 are the same as for the equivalent samples S1, S4, and S5, respectively, since the growth temperatures for the corresponding samples are equal (see Table 1). Moreover, for samples S6, S7, and S8 the indium content was set to 0 after the 4th ML of the LT GaAs cap (the yellow box in Fig. 5c) since the growth temperature (580 °C) of HT GaAs is too high for indium

incorporation. As can be seen on Fig. 5b, the effective bandgap simulation with modified total indium concentration as well as depth-profile for samples S6, S7, and S8 results in the transition energies that are in a good agreement with the experimental PL peak positions. Importantly, the In segregation phenomenon also affects the FWHM of PL peak for samples S1/S4-S8 in Fig. 5a. An explicit trend in the decrease of FWHM of PL peak with decreasing the LT GaAs-cap layer thickness can be observed in Table 1. Consequently, since In(Ga)As QW is not limited to nominal 1 ML thickness due to the In segregation during the GaAs capping, the decrease of the thickness of defective LT-GaAs leads to the decrease of FWHM of PL peak for samples S6-S8. Moreover, for samples S6/S7/S8 there is a good correlation between the FWHM of PL peak and growth temperature of defective LT-GaAs cap. Therefore, the proposed non-destructive PL characterization technique is a powerful tool that can be used to monitor the In segregation in ultra-thin In(Ga)As/GaAs nanostructures. Moreover, such analysis can be applied to predict emission properties for more complicated device-oriented structures such as SML-QD cascade mid-infrared photodetector.

In this work, we presented a simple way to study the In segregation during the GaAs capping process in ultra-thin In(Ga)As/GaAs QWs grown by MBE. The photoluminescence (PL) spectroscopy and the effective bandgap simulation of specially designed ultra-thin In(Ga)As/GaAs nanostructures with the same nominal amount of indium were used to calculate the In segregation coefficient. For InAs, In_{0.5}Ga_{0.5}As and In_{0.25}Ga_{0.75}As QWs with thickness of 1 ML, 2 MLs and 4 MLs, respectively, grown at the same temperature ($T_g^{In(Ga)As} = 460$ °C) the In segregation coefficient was found to be equal $R \sim 0.83$. Moreover, a good correlation of the In segregation coefficient obtained from the proposed method and STEM Z-contrast cross-section imaging is demonstrated. However, unlike the STEM, which is a destructive, expensive, and

time-consuming process, the PL technique is a reliable alternative to probe the indium depth-profiles (indium segregation) in the ultra-thin In(Ga)As/GaAs QW nanostructures. Finally, the possibility of modifying the In depth-distribution profile by tuning the In(Ga)As growth temperature or the thickness of the low-temperature GaAs capping layer was demonstrated.

See the supplementary material for the supporting results of the investigation.

This work was partially supported by the National Science Foundation, grant number 1809054.

DATA AVAILABILITY

The data that support the findings of this study are available from the corresponding author upon reasonable request.

- ¹ X. Sun, P. Wang, T. Wang, L. Chen, Z. Chen, K. Gao, T. Aoki, M. Li, J. Zhang, T. Schulz, M. Albrecht, W. Ge, Y. Arakawa, B. Shen, M. Holmes, and X. Wang, *Light Sci. Appl.* **9**, 159 (2020).
- ² L. Lympirakis, T. Schulz, C. Freysoldt, M. Anikeeva, Z. Chen, X. Zheng, B. Shen, C. Chèze, M. Siekacz, X.Q. Wang, M. Albrecht, and J. Neugebauer, *Phys. Rev. Mater.* **2**, 011601(R) (2018).
- ³ M. Anikeeva, M. Albrecht, F. Mahler, J.W. Tomm, L. Lympirakis, C. Chèze, R. Calarco, J. Neugebauer, and T. Schulz, *Sci. Rep.* **9**, 9047 (2019).
- ⁴ F. Hopfer, A. Mutig, M. Kuntz, G. Fiol, D. Bimberg, N.N. Ledentsov, V.A. Shchukin, S.S. Mikhrin, D.L. Livshits, I.L. Krestnikov, A.R. Kovsh, N.D. Zakharov, and P. Werner, *Appl. Phys. Lett.* **89**, 141106 (2006).
- ⁵ P. Lam, J. Wu, M. Tang, Q. Jiang, S. Hatch, R. Beanland, J. Wilson, R. Allison, and H. Liu, *Sol. Energy Mater. Sol. Cells* **126**, 83 (2014).
- ⁶ D.Z.Y. Ting, S. V. Bandara, S.D. Gunapala, J.M. Mumolo, S.A. Keo, C.J. Hill, J.K. Liu, E.R. Blazejewski, S.B. Rafol, and Y.C. Chang, *Appl. Phys. Lett.* **94**, 111107 (2009).
- ⁷ J. Huang, D. Guo, W. Chen, Z. Deng, Y. Bai, T. Wu, Y. Chen, H. Liu, J. Wu, and B. Chen, *Appl. Phys. Lett.* **111**, 251104 (2017).
- ⁸ S. Harrison, M.P. Young, P.D. Hodgson, R.J. Young, M. Hayne, L. Danos, A. Schliwa, A. Strittmatter, A. Lenz, H. Eisele, U.W. Pohl, and D. Bimberg, *Phys. Rev. B* **93**, 085302 (2016).
- ⁹ C. Chèze, F. Feix, M. Anikeeva, T. Schulz, M. Albrecht, H. Riechert, O. Brandt, and R. Calarco, *Appl. Phys. Lett.* **110**, 072104 (2017).
- ¹⁰ C. Chèze, M. Siekacz, F. Isa, B. Jenichen, F. Feix, J. Buller, T. Schulz, M. Albrecht, C. Skierbiszewski, R. Calarco, and H. Riechert, *J. Appl. Phys.* **120**, 125307 (2016).
- ¹¹ R. Kumar, Y. Maidaniuk, A. Kuchuk, S.K. Saha, P.K. Ghosh, Y.I. Mazur, M.E. Ware, and G.J. Salamo, *J. Appl. Phys.* **124**, 235303 (2018).
- ¹² C. Li, Y. Maidaniuk, A. V. Kuchuk, S. Shetty, P. Ghosh, T.P. White, T. Al Morgan, X. Hu, Y. Wu, M.E. Ware, Y.I. Mazur, and G.J. Salamo, *J. Appl. Phys.* **123**, 195302 (2018).
- ¹³ C. Li, Y. Maidaniuk, A. V. Kuchuk, Y.I. Mazur, M. Benamara, M.E. Ware, and G.J. Salamo, *Mater. Des.* **190**, 108565 (2020).
- ¹⁴ T. Schulz, L. Lympirakis, M. Anikeeva, M. Siekacz, P. Wolny, T. Markurt, and M. Albrecht, *Phys. Rev. Mater.* **4**, 073404 (2020).

- ¹⁵ M. Auf Der Maur, A. Pecchia, G. Penazzi, W. Rodrigues, and A. Di Carlo, *Phys. Rev. Lett.* **116**, 027401 (2016).
- ¹⁶ D. González, V. Braza, A.D. Utrilla, A. Gonzalo, D.F. Reyes, T. Ben, A. Guzman, A. Hierro, and J.M. Ulloa, *Nanotechnology* **28**, 425702 (2017).
- ¹⁷ P.D. Robb, M. Finnie, and A.J. Craven, *Micron* **43**, 1068 (2012).
- ¹⁸ A. Lenz, H. Eisele, J. Becker, J.-H. Schulze, T.D. Germann, F. Luckert, K. Pötschke, E. Lenz, L. Ivanova, A. Strittmatter, D. Bimberg, U.W. Pohl, and M. Dähne, *J. Vac. Sci. Technol. B, Nanotechnol. Microelectron. Mater. Process. Meas. Phenom.* **29**, 04D104 (2011).
- ¹⁹ R. Kumar, Y. Maidaniuk, S.K. Saha, Y.I. Mazur, and G.J. Salamo, *J. Appl. Phys.* **127**, 065306 (2020).
- ²⁰ S.Y. Karpov and Y.N. Makarov, *Thin Solid Films* **380**, 71 (2000).
- ²¹ K. Yamaguchi, T. Okada, and F. Hiwatashi, *Appl. Surf. Sci.* **117/118**, 700 (1997).
- ²² O. Dehaese, X. Wallart, and F. Molloy, *Appl. Phys. Lett.* **66**, 52 (1995).
- ²³ J.M. Moison, C. Guille, F. Houzay, F. Barthe, and M. Van Rompay, *Phys. Rev. B* **40**, 6149 (1989).
- ²⁴ K. Muraki, S. Fukatsu, Y. Shiraki, and R. Ito, *Appl. Phys. Lett.* **61**, 557 (1992).
- ²⁵ M. Ilg, M.I. Alonso, A. Lehmann, K.H. Ploog, and M. Hohenstein, *J. Appl. Phys.* **74**, 7188 (1993).
- ²⁶ R.R. Pelá, L.K. Teles, M. Marques, and S. Martini, *J. Appl. Phys.* **113**, 033515 (2013).
- ²⁷ S. Martini, J.E. Manzoli, and A.A. Quivy, *J. Vac. Sci. Technol. B* **28**, 277 (2010).
- ²⁸ S. Birner, S. Hackenbuchner, M. Sabathil, G. Zandler, J.A. Majewski, T. Andlauer, T. Zibold, R. Morschl, A. Trellakis, and P. Vogl, *Acta Phys. Pol. A* **110**, 111 (2006).
- ²⁹ Z.L. Yuan, Z.Y. Xu, B.Z. Zheng, J.Z. Xu, S.S. Li, W. Ge, Y. Wang, J. Wang, L.L. Chang, P.D. Wang, C.M. Sotomayor Torres, and N.N. Ledentsov, *Phys. Rev. B* **54**, 16919 (1996).
- ³⁰ C. Tran, R. Ares, V. Karasyuk, S. Watkins, G. Letourneau, and R. Leonelli, *Phys. Rev. B* **55**, 4633 (1997).
- ³¹ M.I. Alonso, M. Ilg, and K.H. Ploog, *Phys. Rev. B* **50**, 1628 (1994).
- ³² M.I. Alonso, M. Ilg, K. Ploog, and A. Trampert, *J. Appl. Phys.* **78**, 1980 (1995).
- ³³ U. Pietsch, V. Holý, and T. Baumbach, *High-Resolution X-Ray Scattering* (Springer New York, New York, NY, 2004).
- ³⁴ H. V. Stanchu, A. V. Kuchuk, M. Barchuk, Y.I. Mazur, V.P. Kladko, Z.M. Wang, D. Rafaja,

and G.J. Salamo, *CrystEngComm* **19**, 2977 (2017).

³⁵ H. V. Stanchu, A. V. Kuchuk, P.M. Lytvyn, Y.I. Mazur, Y. Maidaniuk, M. Benamara, S. Li, S. Kryvyi, V.P. Kladko, A.E. Belyaev, Z.M. Wang, and G.J. Salamo, *Mater. Des.* **157**, 141 (2018).

³⁶ C. Bocchi and C. Ferrari, *J. Phys. D. Appl. Phys.* **28**, A164 (1995).

³⁷ P. Wolny, M. Anikeeva, M. Sawicka, T. Schulz, T. Markurt, M. Albrecht, M. Siekacz, and C. Skierbiszewski, *J. Appl. Phys.* **124**, 065701 (2018).

Table 1. Nominal designed and growth parameters of $\text{In}_x\text{Ga}_{1-x}\text{As}$ QWs and LT GaAs-cap layers for samples S1-S8 investigated in the present work.

Sample	$\text{In}_x\text{Ga}_{1-x}\text{As}$ QWs			PL peak FWHM (meV)	LT GaAs-cap thickness (ML)
	composition (x)	thickness N (ML)	T_g^{InGaAs} ($^\circ\text{C}$)		
S1	1	1	460	6.9	35
S2	0.5	2	460	10	35
S3	0.25	4	460	8.6	35
S4	1	1	420	13.6	35
S5	1	1	380	13.5	35
S6	1	1	460	6.4	4
S7	1	1	420	8.2	4
S8	1	1	380	9.3	4

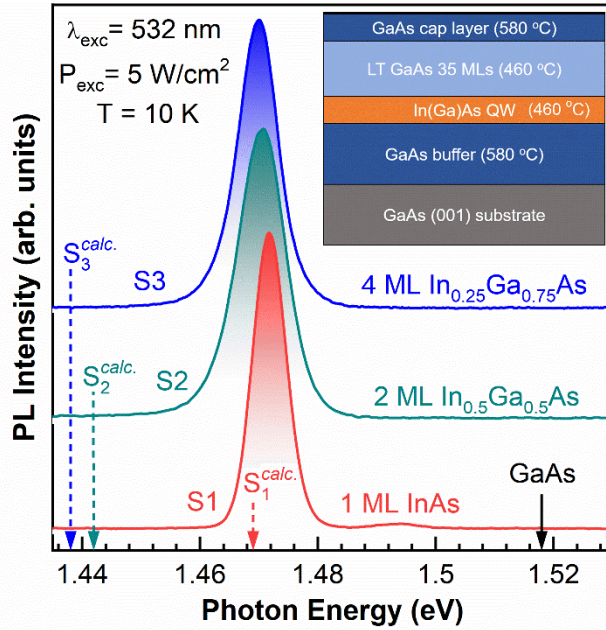


Fig. 1. The low-temperature ($T = 10 \text{ K}$) PL spectra of samples S1, S2, and S3 recorded under the same excitation power intensity ($P_{\text{exc}} = 5 \text{ W/cm}^2$). Vertical dashed lines show calculated ($S^{\text{calc.}}$) transition energies (assuming no In segregation) for corresponding structures. Inset shows the sketch of the samples structure.

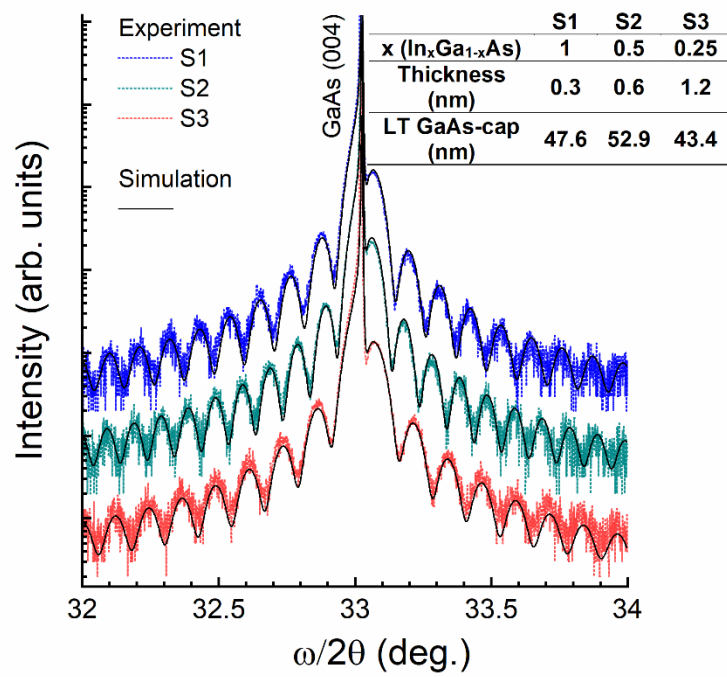


Fig. 2. XRD experimental and fitted $\omega/2\theta$ spectra around GaAs (004) reflections for the investigated S1-S3 samples.

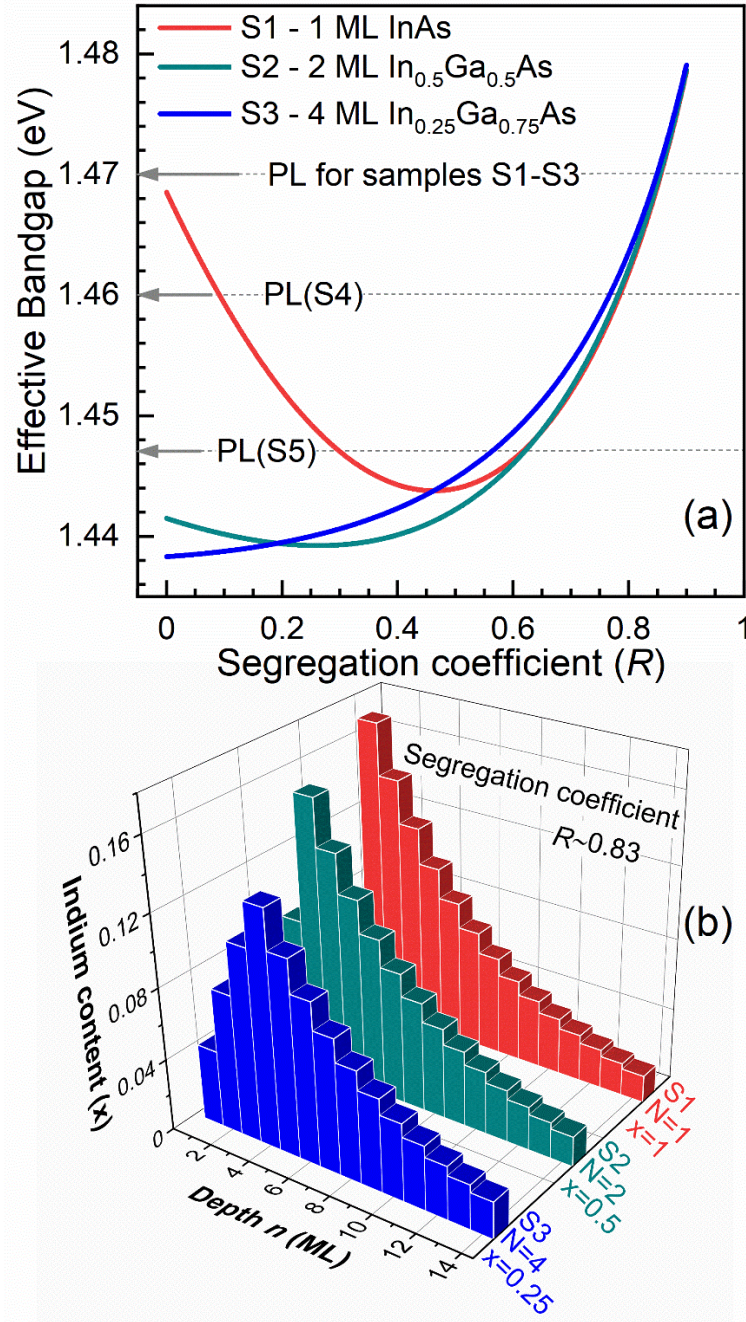


Fig. 3. (a) The simulated effective bandgap (E_g^{eff}) for samples S1-S3 plotted as a function of segregation coefficient (R). The horizontal dashed grey lines show experimental PL peak positions for samples S1-S3, S4 and S5. (b) The resulted indium depth-profiles in In(Ga)As QWs for structures S1, S2, and S3 taking into account the In segregation coefficient $R \sim 0.83$.

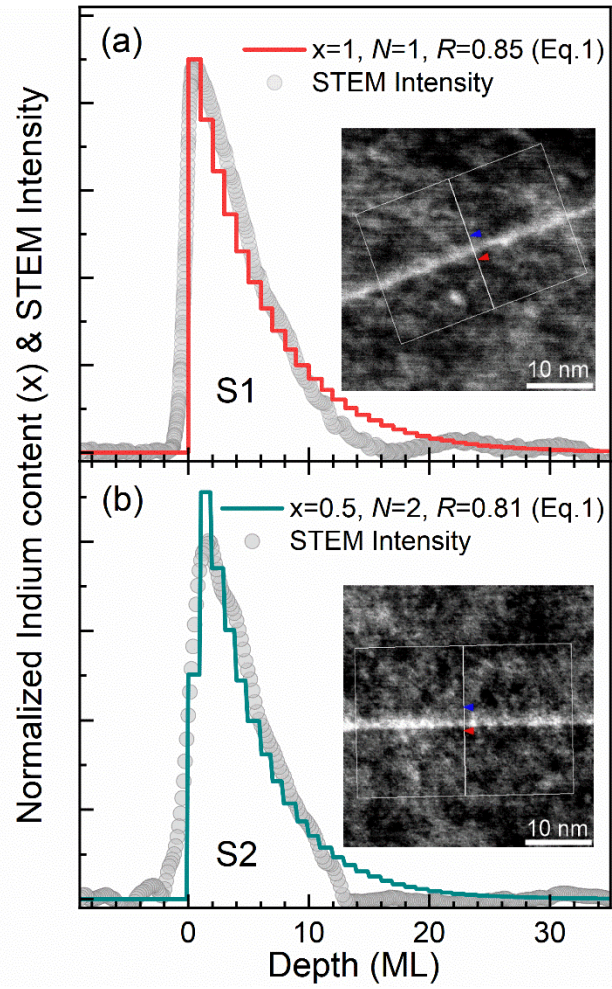


Fig. 4. The normalized indium content and STEM intensity depth-profiles for samples S1 (a) and S2 (b). The insets show actual STEM images of In(Ga)As QW region.

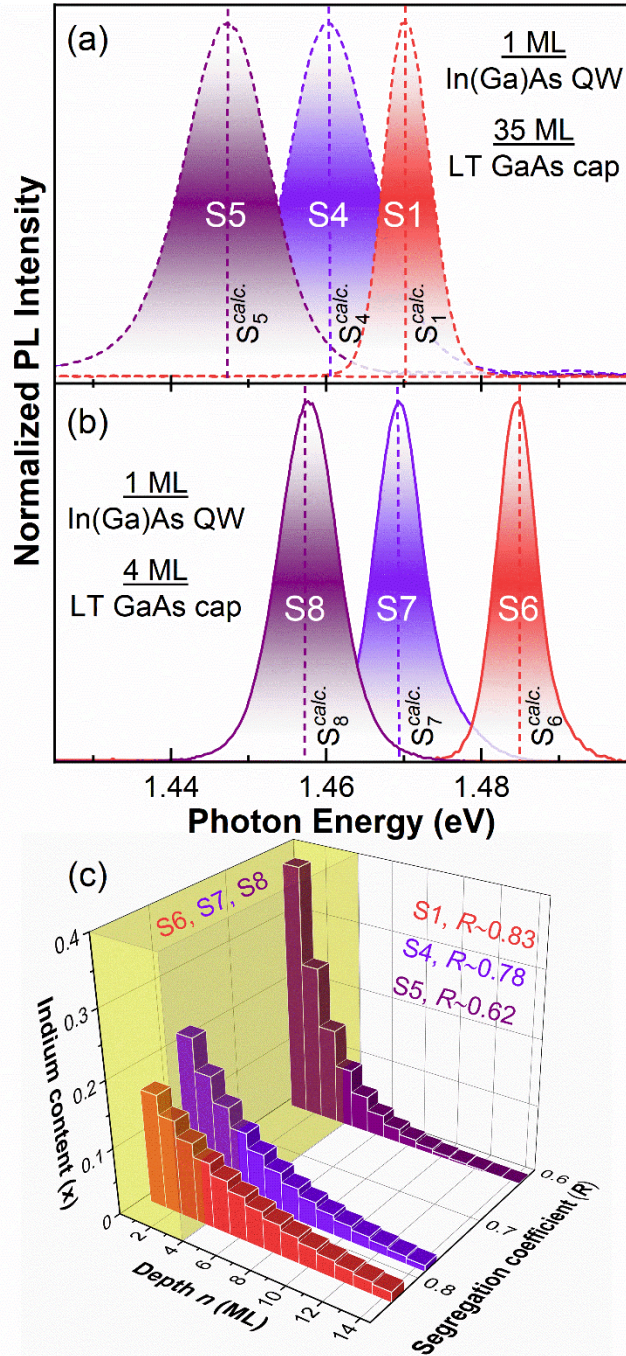


Fig. 5. The normalized PL spectra of the samples S1, S4, and S5 (a) and S6-S8 (b) plotted as a function of photon energy. (c) The indium depth-profiles for samples S1, S4, and S5. The indium depth-profiles from yellow box (In(Ga)As QWs with a limited thickness of 4 MLs) are used to simulate the effective bandgap for samples S6-S8.